3D Polarization properties for crossed-planar undulators

Yuhui Li, Bart Faatz and Joachim Pflueger

Deutsches Elektronen-Synchrotron (DESY), Hamburg, Germany

April 2010, TESLA-FEL 2010-01

3D polarization properties for crossed-planar undulators

Yuhui Li, Bart Faatz, Joachim Pflueger

Deutsches Elektronen-Synchrotron DESY,
Notkestrasse 85, 22607, Hamburg, Germany

Abstract

Instead of using a helical undulator, another method to generate circularly polarized radiation in an FEL is to utilize two crossed planar undulators. The main benefit of the crossed undulator over the helical option is that its structure is simpler. Unlike a helical undulator, two orthogonal polarized fields are respectively generated from two crossed undulators and their combination comprises circularly polarized radiation. Therefore the overlap and resemblance of the two polarizations determine the quality of the composed radiation field.

Simulations have been performed with parameters from the European XFEL in this report. Two algorithms of calculating the stokes parameters for the crossed undulator with emphasis on transverse overlap effects are introduced and compared. The helical properties by crossed undulators are studied in detail.

Key words: XFEL, degree of polarization, stokes parameters, crossed-undulator

1 Introduction

The European XFEL facility will generate radiation wavelengths down to 0.1 nm with a 17.5 GeV electron beam, using Self-Amplified Spontaneous Emission (SASE) [1, 2, 3]. Currently there are three undulator beam lines foreseen: SASE1, SASE2 and SASE3. For 17.5 GeV, SASE1 generates 0.1 nm radiation, SASE2 can generate different wavelengths in the range between 0.1 nm and 0.4 nm by adjusting the undulator gap, SASE3 supplies longer wavelengths from 0.4 nm to 1.6 nm. In the start-up scenario, these three undulator lines consist of planar devices so that only linearly polarized radiation can be generated. While at short wavelengths the linear polarization can be changed into circular radiation by other means, e.g. quarter wave plates, this is not the case for SASE3. Therefore, beyond this start-up scenario, there is a strong wish that SASE3 can also supply circularly polarized light.

To generate circularly polarized light, a natural choice is to use a helical undulator such as an APPLE II. There are practical examples that they can be used for synchrotron radiation [4]. However, there is no example showing how it works for an X-ray FEL. Because the Pierce parameter of an X-ray FEL is very small ($\rho < 10^{-3}$), the undulator tolerance can be expected to be very tight. Whether the technical challenges can be met is still unclear. In addition, helical undulators are much more expensive than planar ones.

An alternative approach is to generate circularly polarized radiation using two crossed planar undulators. It is originally proposed in Refs. [5, 6]. Because the coherence length in SASE FELs is much longer than the coherence length of spontaneous emission, the longitudinal shift between the two fields from two crossed undulators can be made shorter than the coherence length. Thus the combination of the two orthogonal fields results in circular polarization without requiring a complex monochromator which is needed in case of synchrotron radiation due to the lack of longitudinal coherence. With a phase shifter between these two undulators, the polarization can be varied between linear and circular.

Fig. 1 shows the layout of this proposal. In this configuration, electrons successively pass through two crossed planar undulators. The first one is quite long to generate powerful FEL radiation as well as micro-bunch electrons with a periodicity of the radiation wavelength. Because the micro-bunches are already formed in the first undulator, the second undulator emits coherently. Therefore even for a short length of the second undulator powerful FEL radiation comparable in intensity to the radiation by the first long undulator is generated. High degree of circular polarization requires that the radiation powers

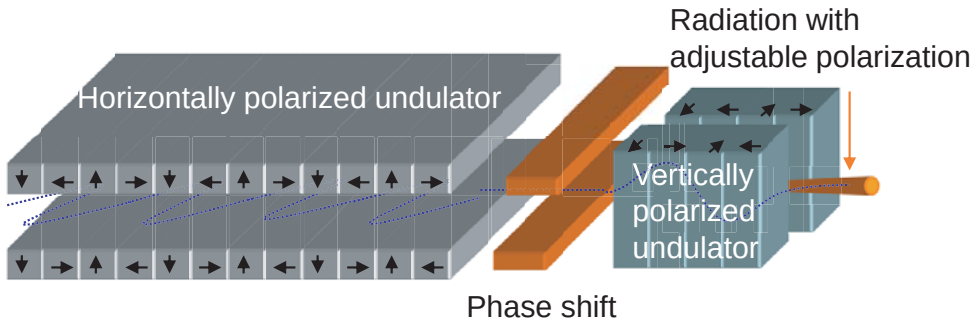

Figure 1: Crossed-planar undulator system for generating high-gain variably polarized FEL radiation as proposed in Refs. [5, 6].

from two undulators are equal. In Ref. [7] it is shown that if the length of the second undulator equals 1.3 gain lengths, the radiation power from the second undulator is equal to the first one. Unfortunately, the gain length is influenced by many parameters such as radiation wavelength, beam current, emittance and β-function. Therefore, this scheme can be optimized for one wavelength with given beam parameters only. For other parameters, the degree of polarization will drop. In addition, the power at the end of the first undulator is not saturated, which causes intrinsic shot-to-shot fluctuation of the intensity. This in turn automatically translates into variation of degree of polarization.

To improve the stability of polarization, a modified scheme has been proposed in Ref [8]. The long planar undulator is only used as a buncher. It is followed by a system to separate the micro bunched electron beam and the linear polarized light. Then it is followed by two equal-length crossed undulators. If the micro bunched structure can be preserved in the separation system, both undulators will coherently radiate and emit the same amount of power as long as the beam parameters do not differ significantly in the two crossed undulators, i.e. if the beam is frozen in phase space. In this case, the two fields should be quite similar so that their combination can be circularly polarized for all wavelengths. Compared to the original scheme, this modification has higher flexibility with respect to undulator length. Fig. 2 shows this modified configuration.

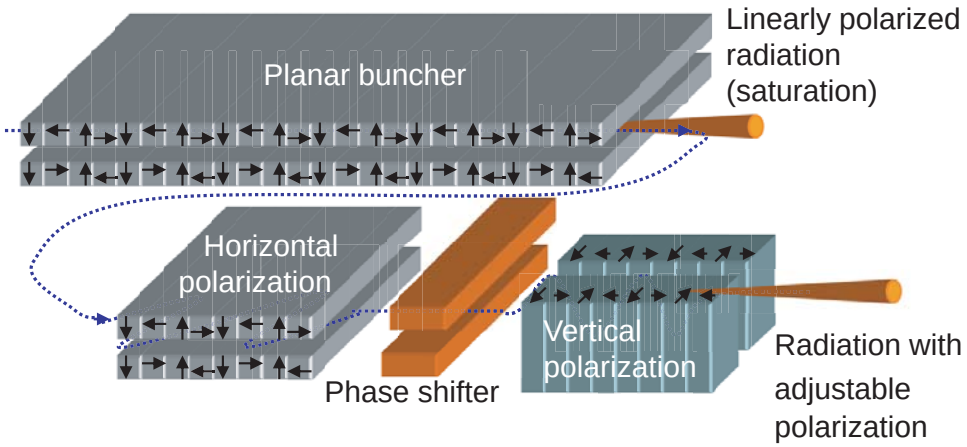

Figure 2: Modified crossed-planar undulator system for generation of variably polarized FEL radiation.

Although the modified scheme in principle can improve the quality of polarization, it is still based on the strategy of combining two separated fields and therefore the polarization can not be perfect. Several points which can decrease its circular polarization can be summarized:

1. The bunching is not frozen in phase space and as consequence, the radiation properties of the two radiators differ slightly.

2. The β-function in this two crossed undulators is not exactly the same, resulting in a different beam size and opening angle.

3. Because of the slippage between electrons and light wave, there is an unavoidable longitudinal shift between the two orthogonal polarized waves generated by two undulators.

4. Because of the different position at which the waves are generated, the two fields' transverse distribution of phase and intensity can not be exactly the same. This difference increases as the two undulators become longer.

The first two points decrease the circular polarization due to a difference in intensity and opening angle or size of two orthogonal field components. The last two reduce the overlap. To include all the points above and calculate the polarization, it is necessary to perform numerical simulations. A 3D FEL simulation code such as Genesis 1.3 [9] can calculate transverse and longitudinal intensity and phase. The simulation can be divided into several steps:

1. Do time dependent simulation of the buncher, dumping the particle distribution file

2. Directly load the particle file dumped by the buncher to the simulations for crossed undulators. This means the impact of bending system is neglected.

3. Do simulations for the two crossed undulators respectively and dump the field files from each of them.

4. Propagate both fields a certain distance in free space (far zone), combine them and calculate the polarization.

The first three steps have been done by the 3D FEL simulation code Genesis [9]. For the fourth step we have tested three different methods to numerically calculate optical field propagation in free space: The spectral method based on FFT, the Fresnel integral method and the straight forward numerical integration of the fields (see Appendix A). Here, we will use the Fresnel method to transport the field to far zone.

In this report, the Stokes parameters are used to describe the polarization properties. In the following section, two algorithms of calculating the stokes parameters are introduced and compared. The polarization versus different longitudinal and transverse shift is studied in detail. In the third section, the polarization dependence on undulator length for different radiation wavelengths is investigated. The fourth section is the summary and outlook. Two appendixes are included: Appendix A compares three different methods for propagating optical wavefront in free space. Appendix B includes some back ground knowledges of the polarization and stokes parameters.

It should be stressed again that the beam dynamics of the system separating the electron beam from the linearly polarized radiation is not included here and is assumed to have no influence on the performance. As such, numbers quoted here for the polarization should be considered upper limits. Study of the arc used to separate the beam from the linearly polarized light is described in [10, 11].

2 Circular polarization properties

2.1 Two algorithms of calculating the stokes parameters from 3D FEL simulation.

The Stokes parameters are generally used to describe a radiation's polarization. They describe the polarization on a specific point. However, in 3D studies the wave's distribution on a transverse plane is always described by a number of points instead of one. Therefore the electric component can be assumed to be $\vec{E}(\vec{r},t)$, where the vector $\vec{r}$ refers to a point's position on the plane.

We can average $\vec{E}(\vec{r},t)$ over a local area:

$$\vec{E}(t) = \frac{1}{s}\int\int_s \vec{E}(\vec{r},t)ds = E_x(t) + E_y(t), \tag{1}$$

where $\vec{E}(t)$ is the average electric component and s denotes the local area around this point. $E_x(t)$ and $E_y(t)$ are the x- and y-components, respectively. How to choose such an area s is crucial and later we will introduce two methods for it. Nevertheless, after obtaining this averaging number, the electric field can be expressed as:

$$\begin{aligned} E_x(t) &= a_1(t)e^{-i[\varpi t-\phi_1(t)]}, \\ E_y(t) &= a_2(t)e^{-i[\varpi t-\phi_2(t)]}, \end{aligned} \tag{2}$$

where ϖ denotes to the mean frequency. $\phi_1(t)$ and $\phi_2(t)$ are the phase of E_x and E_y respectively. The Stokes parameters are defined as:

$$\begin{aligned} S_0 &= \left\langle a_1^2 \right\rangle + \left\langle a_2^2 \right\rangle, \\ S_1 &= \left\langle a_1^2 \right\rangle - \left\langle a_2^2 \right\rangle, \\ S_2 &= 2\left\langle a_1 a_2 \cos(\phi_1 - \phi_2) \right\rangle, \\ S_3 &= 2\left\langle a_1 a_2 \sin(\phi_1 - \phi_2) \right\rangle, \end{aligned} \tag{3}$$

where the bracket $\langle ... \rangle$ denotes the average over time. The total degree of polarization P can be experssed in terms of Stokes parameters:

$$P = \frac{\sqrt{S_1^2 + S_2^2 + S_3^2}}{S_0}. \tag{4}$$

The selection for the integration area s is important. If s is large enough to cover the full transverse plane of the two optical fields from crossed undulators, then all of the simulated $\vec{E}(\vec{r}, t)$ on each point over the transverse plane will be summed up to achieve a general electric component $\vec{E}(t)$. By this means irrespective of the transverse displacement between them, the polarization will be the same. We call this method "integration" method. The Stokes parameters can also be calculated for each point, depending on the vector $\vec{r}$. Adding each of the Stokes parameters with an appropriate weight, one set of Stokes parameters can be obtained. We call this method "differential" method.

In this report, the 3D FEL simulation code Genesis 1.3 is used which describe the optical field with Cartesian coordinate system. As shown in Fig. 3, the whole plane is a square with edge length L. It is divided into $N \times N$ grid points. On each grid point a vector $\vec{E}$ is simulated.

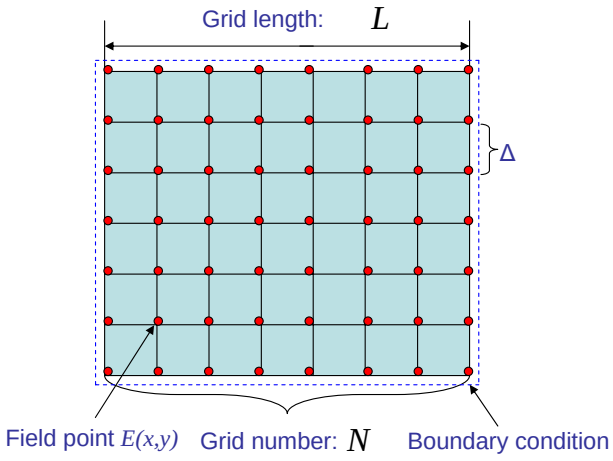

Figure 3: Illustration of the separated field points for numerical simulation.

If the integration method is used, first the general electric component $\vec{E}$ is calculated by summing all points:

$$E_x = \sum_{i=1}^{N\times N} E_{x,i}, \quad E_y = \sum_{i=1}^{N\times N} E_{y,i}. \tag{5}$$

The subscript i denotes to i^{th} point. Then one simply substitutes E_x and E_y into Eqs. (3) (4) to calculate the Stokes parameters and degree of polarization.

If the Differential method is used, first $E_{x,i}$ and $E_{y,i}$ are substituted into Eq. (3) to calculate the Stokes parameters $(S_{0,i}, S_{1,i}, S_{2,i}, S_{3,i})$ for each point. From these parameters, a general Stokes parameters can be calculated:

$$S_0 = I_0, \quad S_1 = I_0 \sum_{i=1}^{N\times N} S_{1,i}W_i, \quad S_2 = I_0 \sum_{i=1}^{N\times N} S_{2,i}W_i, \quad S_3 = I_0 \sum_{i=1}^{N\times N} S_{3,i}W_i. \tag{6}$$

W_i is the weight, it can be calculated from the intensity on each grid point:

$$W_i = \frac{E_{x,i}E^*_{x,i} + E_{y,i}E^*_{y,i}}{\sum_{i=1}^{N\times N}(E_{x,i}E^*_{x,i} + E_{y,i}E^*_{y,i})}, \tag{7}$$

I_0 is the total intensity of the optical field:

$$I_0 = \sum_{i=1}^{N\times N}(E_{x,i}E^*_{x,i} + E_{y,i}E^*_{y,i}). \tag{8}$$

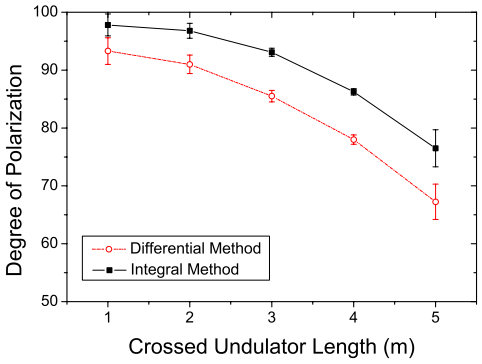

Figure 4: Degree of polarization generated by the crossed undulator. The black solid line refers to the differential method and the red dot line refers to the integration method.

The two methods of calculating stokes parameters will result in different polarizations for the same radiation field. As an example, Fig. 4 shows the polarization of crossed undulators by these two methods. The undulator length is varied from 1 m to 5 m. The simulations are done for 0.4 nm SASE3 of the European XFEL. The black solid line with squaresis uses the differential method and the red dotted line uses the integration method. It is seen that as the undulator length increases, the degree of polarization decreases. Comparing the two methods, for each undulator length, the differential method shows 5 % to 10 % lower polarization than the integration method. The difference is caused by the imprtfext transverse overlap due to a different transverse beam size in the two undulators. The error bar is due to the simulation accuracy.

In the following, the polarization versus different longitudinal and transverse shifts will be discussed by both methods.

2.2 Polarization versus longitudinal shift

SASE FEL radiation contains many spikes in the time domain. Each spike corresponds to a coherence length, but there is no correlation between two spikes, which are therefore are not coherent to each other.

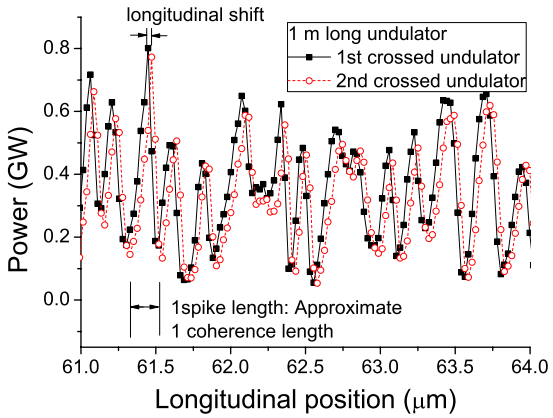

Figure 5: The SASE FEL power distribution in time domain. It is seen that many spikes exist. Each spike corresponds to one coherence length. Due to slippage, the spikes are longitudinally shifted. In this plot, each crossed undulator length is 1 m.

Because electrons are slower than light, the fields generated by the two undulators have a small longitudinal shift. The shift length is equal to the number of undulator periods multiplied by the wavelength. Fig. 5 shows this phenomenon. Because a high degree of polarization requires that the two fields add up coherently, it is clear that the longitudinal shift reduces the degree of polarization. Therefore it is important to study how the polarization drops with increased longitudinal shift.

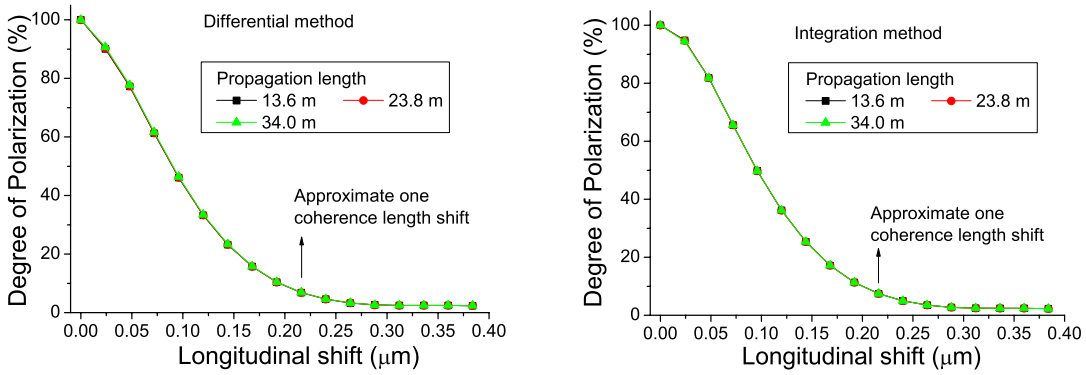

Figure 6: Polarization versus longitudinal shift between two orthogonal fields. The two beam's intensity and phase distribution are exactly the same. Because the degree of polarization is independent of propagation length, the three curves are on top of each other. The left plot is the result by differential method and the right plot is the result by integration method.

Beside longitudinal shift, there are other effects which can also decrease polarization. Therefore to focus on the impact of longitudinal shift, we select two exactly identical fields. In simulations, the longitudinal shift can be artificially changed and different corresponding polarization states can be calculated. Fig. 6 shows the result. When the longitudinal shift is zero the polarization is 100 %. This is because the two fields are identical. As the longitudinal shift increases, the degree of polarization drops. When the shift is larger than one coherence length (full length of one spike), the polarization drops to almost zero. This simulation result is consistent with the analysis above. In addition, for each longitudinal shift, three different distances from the source have been simulated in order to check numerical accuracy, namely 13.6, 23.8 and 34 m. As expected, they show virtually identical results and are indistinguishable in Fig. 6.

The integration and differential methods show quite similar result here, the only difference is that the differential method shows faster decrease of degree of polarization.

2.3 Fluctuation of polarization

The spiky structure of a SASE FEL is caused by random shot noise. Therefore the polarization changes from shot to shot. In order to simulate this, rather than performing many simulations to get the statistics, the longitudinal beam distribution is described by a water-bag, e.g. a homogeneous, instead of a Gaussian distribution. We can now select a part of the whole beam and calculate the polarization for this fraction only. The part of the beam which we select, in the remainder of this paper referred to as sub-beam, can be chosen in length and position. By this means we can get some information on polarization fluctuations.

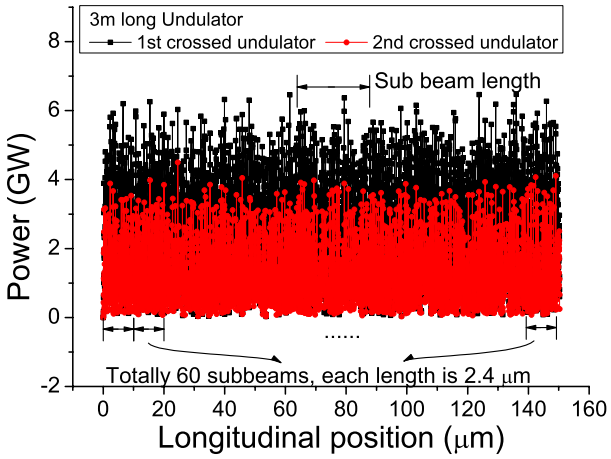

Figure 7: Power distribution in time domain. The beam profile is homogeneous with a peak current of 5 kA. The simulated length of 144 μm can be divided into many sub-beams. The length analyzed can be adjusted.

Because two identical fields will always have perfect polarization, independent of what length we choose, i.e. what sub-beam we take, we choose them to be slightly different in this section. They are calculated from two 3 meter long crossed undulators. Fig. 7 illustrates this. It is seen that hundreds of small spikes are included in the beam.

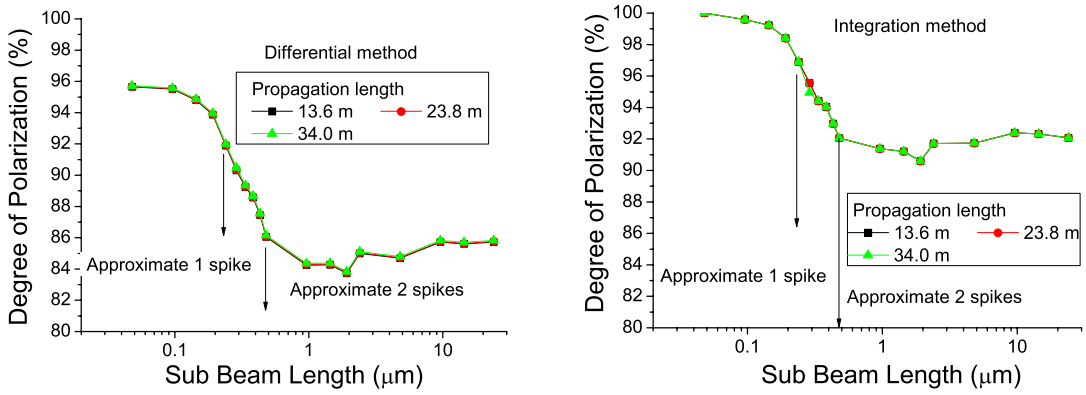

Figure 8: The degree of polarization versus different sub-beam lengths. The sub-beam is always taken around the center part of the whole beam. The left plot uses the differential method and the right plot is the result by integration method.

We can first investigate how the degree of polarization changes with different sub-beam lengths by lengthening our window of observation from a single coherent spike to several spikes. Fig. 8 shows the result. It is calculated from the sub-beam window which is always kept in the middle of the whole beam.

From this Figure, it is seen that as long as the window which we consider is shorter than a coherence length, the degree of polarization is high. As the window increases, the degree of polarization drops. After the sub-beam involves more than two spikes (longer than two coherence lengths), the decrease stops and it keeps varying within several percent range. In this simulation three different propagation lengths from 13.6 to 34 m have been calculated, all showing virtually identical behavior. Except that the differential method shows in general a lower degree of coherence, the drop in coherence is independent of the model used.

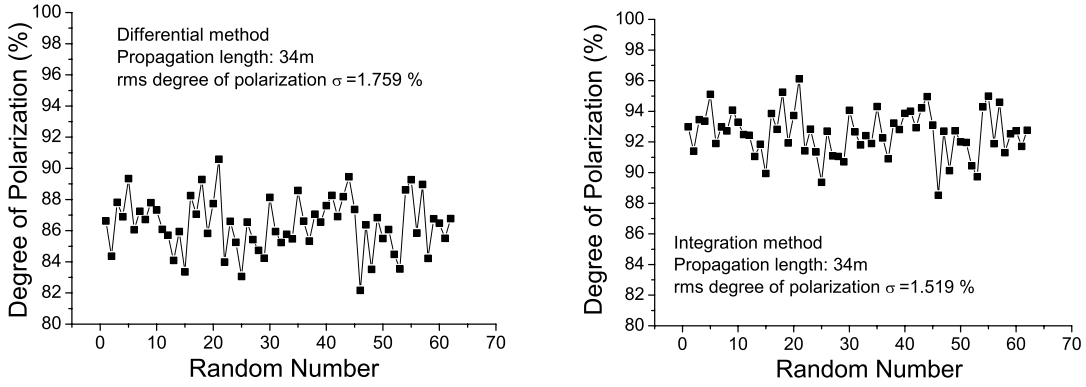

Figure 9: Shot to shot variation of polarization. Each sub-beam's length is 2.4 μm (8 fs). Totally 60 sub-beams are simulated. The left plot is the result by differential method and the right plot is the result by integration method.

The fluctuation in polarization is checked by dividing the whole beam into 60 sub-beams, each with a length of about 2.4 μm, i.e. 8 fs. (see Fig. 7), Fig. 9 shows the result. It is seen that both of the methods foresee the similar RMS fluctuation of polarization, a little larger than 1.5 %. In this simulation, the fluctuation only comes from random shot noise of SASE FEL. Other sources such as instability of electron beam are not taken into account. Therefore this fluctuation is only a minimum value, more detailed investigation is needed but beyond the study in this paper. The differential methods shows about 6% lower average polarization than the integration method.

2.4 Polarization versus transverse displacement

In this subsection we study the influence by the two beams' transverse displacement. If the electron is kicked in the crossed undulator or in the intersection between them, there will be an offset between the two optical fields. Because here we want to focus on the influence by transverse displacement, two exactly same beams are selected for the simulation. By this means, other influences to the polarization can be avoided.

First we transport these two beams from the exit of crossed undulator to far zone. The propagation length is 13.6 m. Then the two beams are artificially displaced. δ_x and δ_y are used to denote the offset in x- and y- direction, respectively. By scanning different δ_x and δ_y, the degree of polarization versus offset can be studied. To clearly show how the two fields are transversely separated, Fig. 10 shows as an example the intensity distribution over a transverse plane. The offsets are $\delta_x = \delta_y = 106\mu m$.

Fig. 11 shows the simulated degree of polarization. The left plot uses the differential method. It is seen that as the offset increases, the degree of polarization continuously drops. When δx and δy are larger than 50 μm the degree of polarization is zero. The right plot in Fig. 11 is the simulation result by integration method. It shows totally different behavior as the differential methods: independent how large the δx and δy are, the circular polarization is always 100 %. As the introduction above, the integration method first summing up all beams on every grid point over the whole plane. Therefore the offset, no matter how large it is, does not influence the result at all. Contrary to this, the differential method first calculates the degree of polarization one each grid point. If the two fields do not overlap, the degree of

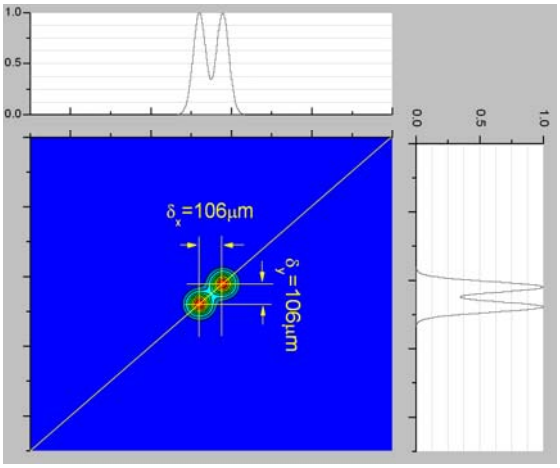

Figure 10: Intensity distribution of the optical field consisting of two parts with an offset.

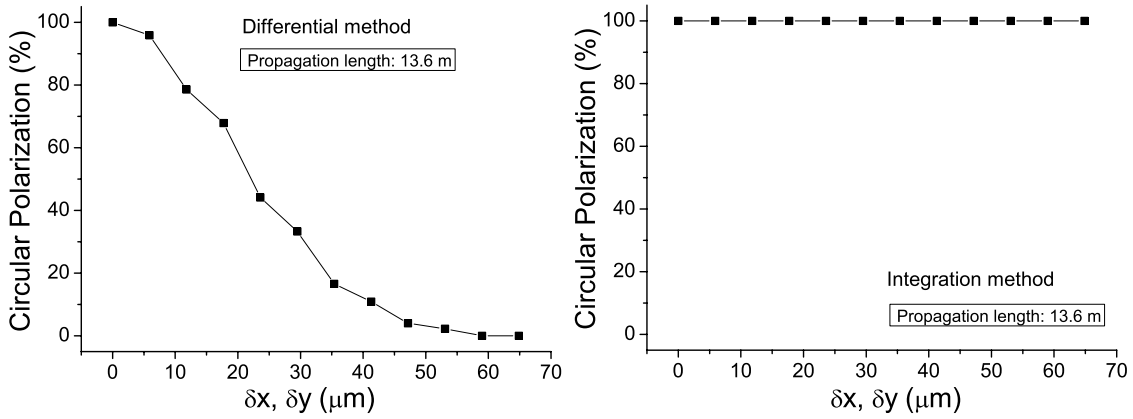

Figure 11: Circular polarization versus different transverse offsets δx and δy. The left plot is the result by the differential method and the right plot is the result by integration method.

polarization would be poor on each grid point. Hence the general polarization from them becomes lower as the offset increases.

2.5 Polarization versus transverse plane size.

In this subsection we study the polarization versus different transverse sizes. Imagining that there is an aperture in the beam line, only a part of the radiation is permitted to pass through it. Then how the polarization varies versus the aperture size is interesting to study.

In the simulations we always fix the aperture center superposing with the radiation center. Unlike the simulations for transverse mis-overlap, where the two radiation components are exactly the same, here we choose two components emitted from two 3 m long crossed undulators, respectively. If the two fields were exactly the same, the polarization will always be 100 %, independent of the aperture size.

Fig. 12 shows the results. Before calculating the degree of polarization, the two components are respectively transported three different lengths. The left plot is the result by differential method and the right plot is the result by integration method. It is seen that when the differential method is used, as the aperture size increasing the degree of polarization drops until the aperture is larger than a critical size to pass full radiation go through it. Then the degree of polarization will fix at a certain value. Because the longer the radiation propagates the larger transverse size it is, for a longer transporting length, the aperture's critical size is larger. However, the bottom plot shows a totally different phenomenon: The

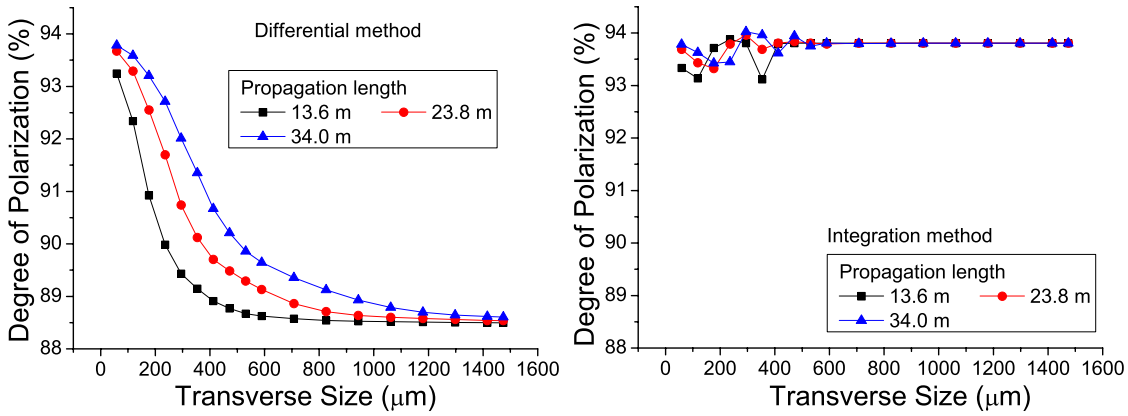

Figure 12: The degree of polarization for different transverse integration sizes and different propagation lengths. The left plot adopts the differential method and right plot the integration method.

aperture size doesn't influent the degree of polarization much. When the size is small, it just oscillate a little and when the size is large, the polarization is quite fixed.

From the introduction for the differential method and integration method, when the aperture size is very small, the two methods actually are the same. Therefore it is seen from Fig. 12 that at small aperture size, the two methods give same degree of polarization. The degree of polarization droppoing shown for differentiation method corresponds to its lower polarization than the integration method shown in Fig. 4.

3 Circular polarization for different wavelengths and different undulator lengths

In this section, we want to focus on some optimization studies. All of the simulations in this section adopt the integration method.

Difference between two polarization components can reduce the circular polarization. For short crossed undulators, the resemblance of two components is better, but at lower radiation power. Therefore an optimization study for crossed undulator length is necessary. SASE3 will supply wavelength adjustable radiation (0.4-1.6 nm). So we should scan over all different wavelengths and calculate their radiation powers and Stokes parameters. This has to be repeated for several lengths of the undulators.

The SASE3 undulator is gap adjustable. Therefore, for simplification we choose $K_{rms} = 3.58$, 5.16, 6.36, 7.36, respectively, corresponding to the foreseen wavelength change by gap variation from 0.4 nm to 1.6 nm. The length of the first long undulator (bunching undulator) is chosen such that the electron micro bunching is closest to the maximum value. For each wavelength, five different crossed undulator lengths from 1 m to 5 m are simulated, where 5 m is approximately one gain length at 0.4 nm. As already mentioned, before combining the two optical field components to calculate the polarization, they are transported over a long distance in free space from the source point (end of undulator) to the observation point. The propagation length is long enough that the beam size expands linearly with distance (far field approximation), corresponding to approximately 30 m in our case. Due to the field expansion, we set an aperture of 4 mm at the observation point to permit all radiation power to pass through. Because the phase shifter value is adjustable, to achieve a maximum value of $|S_3/S_0|$, we always optimize it such that $|S_2|$ has its smallest value. If the two fields are exactly the same when they are combined, the optimized value for the phase difference should be $\pi/2$ (See definition Eq. (3)). Since the amplitudes of the fields generated by the two undulators are different and the propagation distance differs by at least one undulator length, the actual value of the phase shift differs from $\pi/2$. Finally, a SASE FEL shows random spikes distributed in time domain. In order to include more spikes and thus get more statistics, we take a 150 μm long bunch with homogeneous current distribution instead of a 25 μm long Gaussian bunch. Table. 1 lists the main parameters used in our simulations.

Table 1: Parameters for SASE3 used in simulation

Parameter	**Value**
Undulator period λ_u (mm)	68
Undulator parameter K_{rms}	3.58-7.36
Segment length (m)	5
Electron beam energy (GeV)	17.5
Radiation wavelength (nm)	0.4-1.6
Energy spread (MeV)	8.0
Bunch current (flat top in kA)	5
Bunch length (μm)	150
Normalized emittance (mm mrad)	1.4

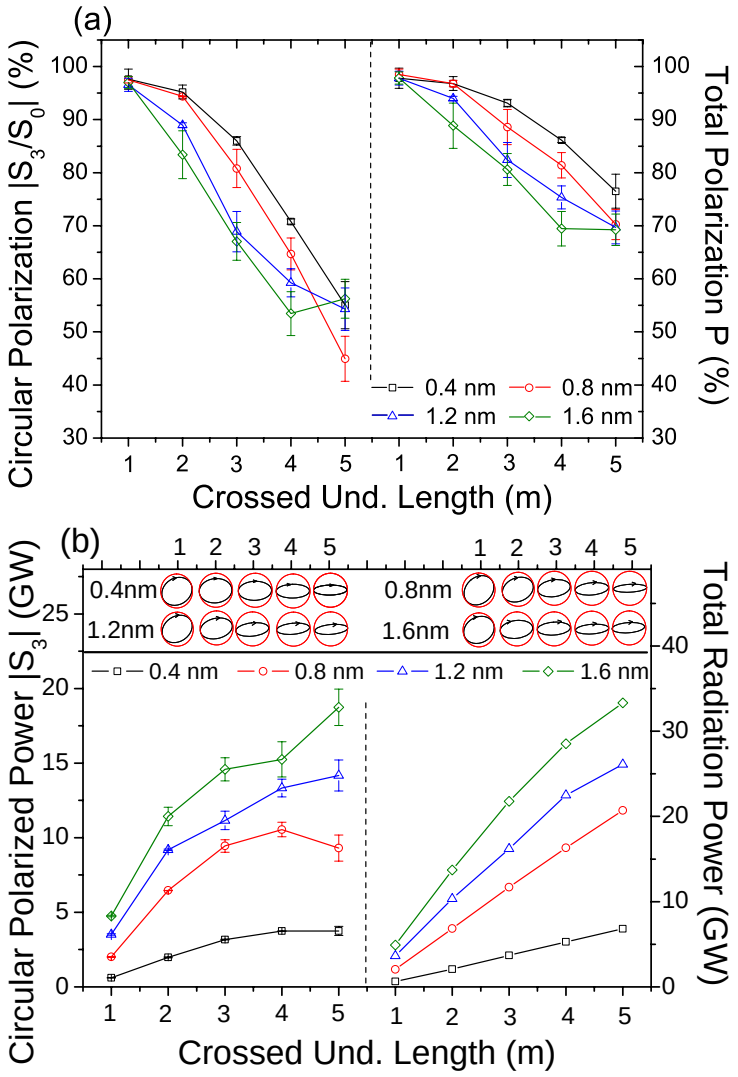

Figure 13: Top: Circular polarization (left) and total polarization (right). Bottom: circular polarized power (right), total power (left). The polarization ellipses are shown for illustration.

Fig. 13 illustrates the the polarization $|S_3/S_0|$ (top left), total degree of polarization (top right), the radiation power of circularly polarized radiation $|S_3|$ (bottom left) and the radiation power (bottom right) and the polarization ellipse. It is seen that as the crossed undulator length increases, both the degree

of polarization and $|S_3/S_0|$ go down, while the latter one decreases more. This can be understood as follows: Because of the increased undulator length, the slippage between both fields becomes larger as well and hence the longitudinal overlap of different spikes decreases both the degree of polarization and its fraction of circular polarization. The fraction of circularly polarized radiation decreases even more because at longer undulator length beam dynamics plays a more prominent role. Therefore also the increased energy spread (and therefore the difference in power level in the second undulator) diminishes the circular fraction in addition. We can see that at the shortest crossed undulators length of 1 m, a total degree of polarization of more than 95 % and circular polarization of $|S_3/S_0|$ can be expected. On the other hand, however, we also noticed that the radiation power increases for longer undulators. Therefore, the polarized power $|S_3|$ should be used as an alternative figure of merit to be defined by an experiment. From Fig. 13, only a crossed undulator length of up to 4 m gives a significant increase in circular polarized power $|S_3|$. From the bottom left plot, for example for the shortest wavelength of 0.4 nm and an undulator length of 3 m, the circular radiation power is nearly 4 GW. For comparison the FEL power of the planar SASE3 undulator is about 49 GW. If it would be built using helical APPLE II type segments, the power level would be similar. Thus a crossed undulator scheme with 3 m long structures can deliver a maximum circular polarized power of about 10% of what a purely helical undulator can deliver.

4 Summary and Outlook

In this report a 3D simulation method for calculation of polarization properties of a crossed planar undulator was discussed. Because the circular polarization is obtained by combining two individually orthogonal linearly polarized fields, the circular polarization can not be perfect. In general, the reduction of circular polarization mainly has two reasons, one is because the two fields are not exactly the same, the other is because of the slippage. The first effect stems from radiation properties. It can be simulated by a 3D FEL simulation code such as Genesis 1.3. The second effect can be investigated by properly combining the two field components to calculate the polarization.

In order to study the polarization in detail the Fresnel method was applied to study the beam properties in far zone approximation. In this way polarization properties were studied as a function of different longitudinal overlap. Finally the polarization properties were studied as a function of undulator length for wavelengths ranging from 0.4 nm to 1.6 nm.

The optimum length of the two crossed undulators was found to be between 3 and 4 meters. For lengths exceeding 4 m, the total radiation power increases but the circular fraction remains constant. For undulator lengths below 3 m, the degree of circular polarization increases from 70-90% (depending on the wavelength) to close to 100%, but at the expense of a much lower power. Because of the longer gain length at shorter wavelengths, the shorter wavelengths clearly benefit more from the longer undulator length because the fraction of circular polarization remains higher.

So far this paper focused only on the radiation properties of a crossed undulator, which is well separated from the field of the bunching undulator. Electron optics were not considered so far. The micro bunching obtained in the planar SASE3 undulator needs to be preserved and transported throughout the bending section, which is needed to separate the beam to the beginning of the crossed undulator, see Fig. 2. In order to preserve FEL properties, micro bunching has to be preserved on a length scale smaller than the radiation wavelength λ_r. This requires an achromatic and isochronous bend. In first (linear) order such a bending system requires three dipoles with opposite bending radii and two quadrupoles, which are arranged in a mirror symmetric geometry. In addition initial conditions on the electron optic functions $\alpha_{x,y}$ and $\beta_{x,y}$ at the begin of the bending section have to be fulfilled [10]. In linear order such a bend system was already shown to work for micro bunch lengths $\lambda_r > 1$ nm. For preserving even smaller micro bunch lengths higher order aberrations have to be corrected, which require non-linear elements, such as sextupoles and substantially more effort. Detailed studies are underway and will be presented a later publication [11]. The results of ref. [10], however, are encouraging and demonstrate that a crossed undulator as presented in this report is feasible.

ACKNOWLEDGMENTS

We thank Dr. Peter J.M. van der Slot and Dr. Y. Ding as well as Dr. E. Saldin for many useful discussions.

Appendix A: Numerical calculation of paraxial radiation propagation

We do the simulation by a generally used FEL 3D code Genesis 1.3 which delivers the radiation wavefront at the end of undulator [9]. In Genesis 1.3 Cartesian coordinates are used: $\vec{r}_j \equiv \vec{r}_{n(j),m(j)} = (n(j)\Delta)\hat{e}_x + (m(j)\Delta)\hat{e}_y$, where $\hat{e}_{x,y}$ are unit vectors in the x- and y-direction respectively, Δ is the separation of two adjacent grid points and $(n(j), m(j))$ are the grid points. As long as the Δ is suitably chosen, high field transverse modes can be included.

The wave equation with paraxial approximation in a free space is:

$$\nabla_\perp^2 E - 2ik_r\frac{\partial E}{\partial z} = \frac{\partial^2 E}{\partial x^2} + \frac{\partial^2 E}{\partial y^2} - 2ik_r\frac{\partial E}{\partial z} = 0, \tag{9}$$

where $k_r = 2\pi/\lambda_r$, λ_r is the radiation wavelength and E is the electric field.

A.1 Spectral Method (Fourier Transformation)

One generally used propagation method uses the Fourier transform:

$$\tilde{E}(k_x, k_y, z) = \int_{-\infty}^{\infty} dx \int_{-\infty}^{\infty} E(x, y, z)e^{-i(k_x x + k_y y)}dy, \tag{10}$$

where $\tilde{E}$ is the electric field component transformed into frequency domain. Combining Eqs. (9) and (10) and because k_x and k_y are independent of x and y:

$$(k_x^2 + k_y^2)\tilde{E} - 2ik_r\frac{\partial \tilde{E}}{\partial z} = 0. \tag{11}$$

This equation is the wave function in frequency domain. Compare Eqs. (11) and (9) the transverse partial differential $\nabla_\perp^2$ disappears and it is just a first order differential equation, which can be solved analytically:

$$\tilde{E}(k_x, k_y, z) = \tilde{E}(k_x, k_y, 0)e^{-i\frac{k_x^2 + k_y^2}{2k_r}}. \tag{12}$$

Applying the inverse Fourier transform to Eq. (12), the electric component at position z can be found:

$$E(x, y, z) = \frac{1}{4\pi^2}\int_{-\infty}^{\infty} dk_x \int_{-\infty}^{\infty} \tilde{E}(k_x, k_y, z)e^{i(k_x x + k_y y)}dk_y. \tag{13}$$

The equations above are analytical solutions. In numerical simulations the integration of the Fourier transform is replaced by summing up separated values. Fig. 14 shows the distribution of $E(x, y)$ expressed by a series of individual complex values on a plane. As shown in Fig. 14 the field size is the Grid length L and the grid point number is N, the distance between two neighboring points is Δ and $\Delta = L/N$. The Fourier transform equation in this case is [13]:

$$\tilde{E}(k_x, k_y) = \sum_{n_x=0}^{N-1}\sum_{n_y=0}^{N-1} \exp(2\pi i k_x n_x/N)\exp(2\pi i k_y n_y/N)E(n_x, n_y), \tag{14}$$

where $n_x = 0, 1, ..., N-1$ and $n_y = 0, 1, ..., N-1$ represent the transverse position on the plane. $k_x = 0, 1, ..., N-1$ and $k_y = 0, 1, ..., N-1$ represent the parameters in the frequency domain. The inverse Fourier transform equation is:

$$E(n_x, n_y) = \frac{1}{N^2}\sum_{k_x=0}^{N-1}\sum_{k_y=0}^{N-1} \exp(-2\pi i k_x n_x/N)\exp(-2\pi i k_y n_y/N)\tilde{E}(k_x, k_y). \tag{15}$$

In the numerical Fourier transformation, the two dimensional Fast Fourier Transformation (FFT) is normally used.

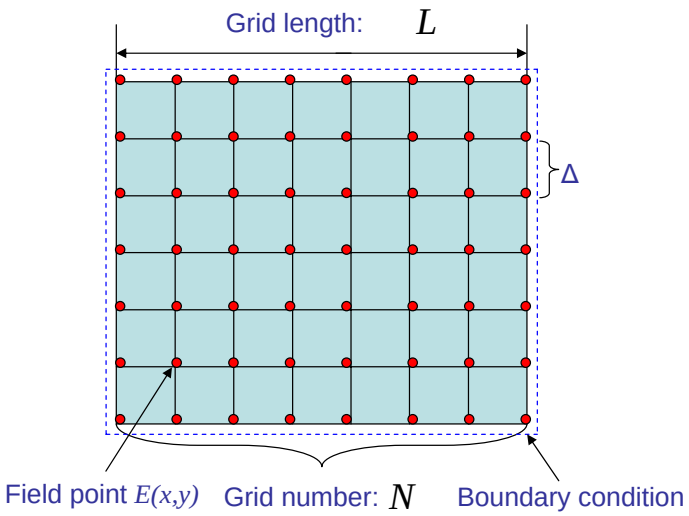

Figure 14: Illustration of the separated field points for numerical simulation.

A.2 Fresnel Integral

The Fresnel Diffraction Integral method can be obtained from Huygens' integral by applying the paraxial approximation. The transverse field at position z can be expressed by integration over the plane at the original position $z = 0$:

$$E(x, y, z) = -\frac{i}{\lambda_r z} \int_{-\infty}^{\infty} \int_{-\infty}^{\infty} E_0(\xi, \eta) e^{i\frac{k_r}{2z}[(x-\xi)^2+(y-\eta)^2]} d\xi d\eta, \tag{16}$$

where $E_0(\xi, \eta)$ expresses field distribution on the initial plane. From Eq. (16), it can be found that in numerical integration, to calculate each point at final plane, N^2 terms must be summed. The meaning of N is shown in Fig. 14. Therefore, the total number of calculations is N^4, which requires too much computing time. The requirement can be reduced by assuming that the diffraction in each direction is independent. Thus the 2D integration can be reduced to be two times of 1D integration.

$$E(x, y, z) = \int_{-\infty}^{\infty} \sqrt{\frac{1}{i\lambda_r z}} e^{i\frac{k_r}{2z}(y-\eta)^2} E(\xi, \eta) d\eta, \quad E(\xi, \eta) = \int_{-\infty}^{\infty} \sqrt{\frac{1}{i\lambda_r z}} E_0(\xi, \eta) e^{i\frac{k_r}{2z}(x-\xi)^2} d\xi. \tag{17}$$

Since each 1D integration is proportional to N^2, the total amount is reduced to be $2 \times N^2$. Moreover, the 1D integration can be solved by using the convolution method:

$$\int_{-\infty}^{\infty} \sqrt{\frac{1}{i\lambda_r z}} e^{i\frac{k_r}{2z}(y-\eta)^2} E(\xi, \eta) d\eta = \sqrt{\frac{1}{i\lambda_r z}} e^{-i\frac{k_r}{2z}y^2} \otimes E(\xi, \eta), \tag{18}$$

and

$$\int_{-\infty}^{\infty} \sqrt{\frac{1}{i\lambda_r z}} E_0(\xi, \eta) e^{i\frac{k_r}{2z}(x-\xi)^2} d\xi = \sqrt{\frac{1}{i\lambda_r z}} e^{-i\frac{k_r}{2z}x^2} \otimes E_0(\xi, \eta). \tag{19}$$

In the 1D convolution, the FFT method can be used to improve the calculation speed:

$$f \otimes g = F^{-1}(F(f)F(g)), \tag{20}$$

where F denotes to the Fourier transform.

A.3 Direct integration

An alternative method to do the propagation calculation is to directly solve Eq. (9). The transverse partially differential can be calculated as:

$$\nabla_{\perp}^2 E = \frac{E_{n_x+1,n_y} + E_{n_x-1,n_y} + E_{n_x,n_y+1} + E_{n_x,n_y-1} - 4E_{n_x,n_y}}{\Delta^2}, \tag{21}$$

where E_{n_x,n_y} means the electric component on the point of n_x, n_y. For each integration step on z-direction, the electric component $E(n_x, n_y)$ is known, so the Laplace operator $\nabla_{\perp}^2$ can be calculated by Eq. (21). For all of the grid points, $\nabla_{\perp}^2$ can be represented by a matrix ζ. Several different boundary conditions can be included when we calculate the matrix ζ. Therefore the solution of wave equation Eq. (9) is:

$$E^{(m+1)} = E^{(m)} + i\frac{\Delta z}{2k_r}\zeta\left[E^{(m)}\right], \tag{22}$$

where the superscript (m) means the mth integration step.

By this way the field propagation can be performed. Compare to the Fourier transform method, the calculation amount is larger. On the other hand, the choice of boundary condition is also important.

A.4 Comparison of the three methods

To compare these three methods a Gaussian beam is transported in free space. The propagation can be performed by numerical simulation of the three methods mentioned above as well as by analytical calculation. The normalized field pattern of a Gaussian beam at any plane z will be expressed by:

$$\tilde{E}(x,y,z) = \left(\frac{2}{\pi}\right)^2 \frac{\exp[-jk_r z + j\psi(z)]}{w(z)} \exp\left[-\frac{x^2+y^2}{w^2(z)} - jk_r\frac{x^2+y^2}{2R(z)}\right], \tag{23}$$

where the beam transverse size $w(z)$, the radius of curvature $R(z)$ and the phase $\psi(z)$ can be related to the waist spot size w_0 and Rayleigh length:

$$w(z) = w_0\sqrt{1+\left(\frac{z}{z_R}\right)^2}, \quad R(z) = z + \frac{z_R^2}{z}, \quad \psi(z) = \tan^{-1}\left(\frac{z}{z_R}\right), \tag{24}$$

where the waist is choosen at $z = 0$.

Based on Eqs. (23) and (24), a Gaussian beam is selected to be transported by different methods. Its wavelength is 0.4 nm, Rayleigh length is $z_R = 2$ m, the initial longitudinal position is $z = 20$ m, the waist spot size is $w_0 = 25$ μm. Fig. 15 shows the beam's transverse distribution.

To compare the properties of these three methods, Fig. 16 shows the intensity distribution in the transverse plane. The field propagation is simulated by the three numerical methods as well as by the analytical solution for comparison. The different plots corresponds to different propagation lengths. In plot (a), the propagation length is the shortest 1.95 m, in plot (b) the propagation length is 32.5 m and in plot (c) the propagation length is longest 97.5 m. In plot (a), two mesh numbers have been chosen for Fresnel method. If the transverse pattern is described by 151×151 points, the Fresnel method shows oscillations,which is not correct. With more grid points, 900×900, its result is consistent with the other methods, which is considered to be correct. The grid number for spectral and direct integration methods are fixed to be 151×151. From this plot, it is concluded that for a short length propagation, both spectral and direct integration methods can give correct results with relatively small number of mesh points while the Fresnel method needs more mesh points to make its result correct. In plot (b), the propagation length is 32.5 m, the mesh number is 151×151. It is seen that all of the three methods are in agreement with the analytical result. In plot (c), the propagation length is 97.5 m, the mesh number is 151×151. It is seen that only the Fresnel method agrees with analytical solution, both of spectral method and direct integration method have not accurate results. The reason is because the transverse size for the calculation is not large enough.

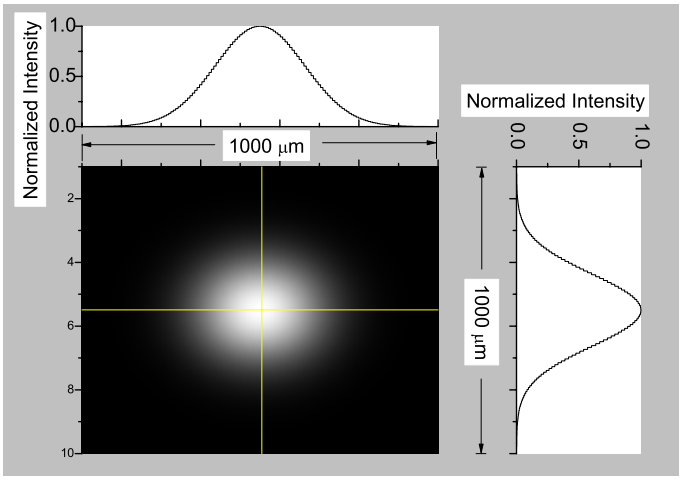

Figure 15: Initial Gaussian field. The wavelength is 0.4 nm, Rayleigh length is $z_R = 2\ m$, the initial longitudinal position is $z = 20\ m$, the waist spot size is $w_0 = 25\ \mu m$.

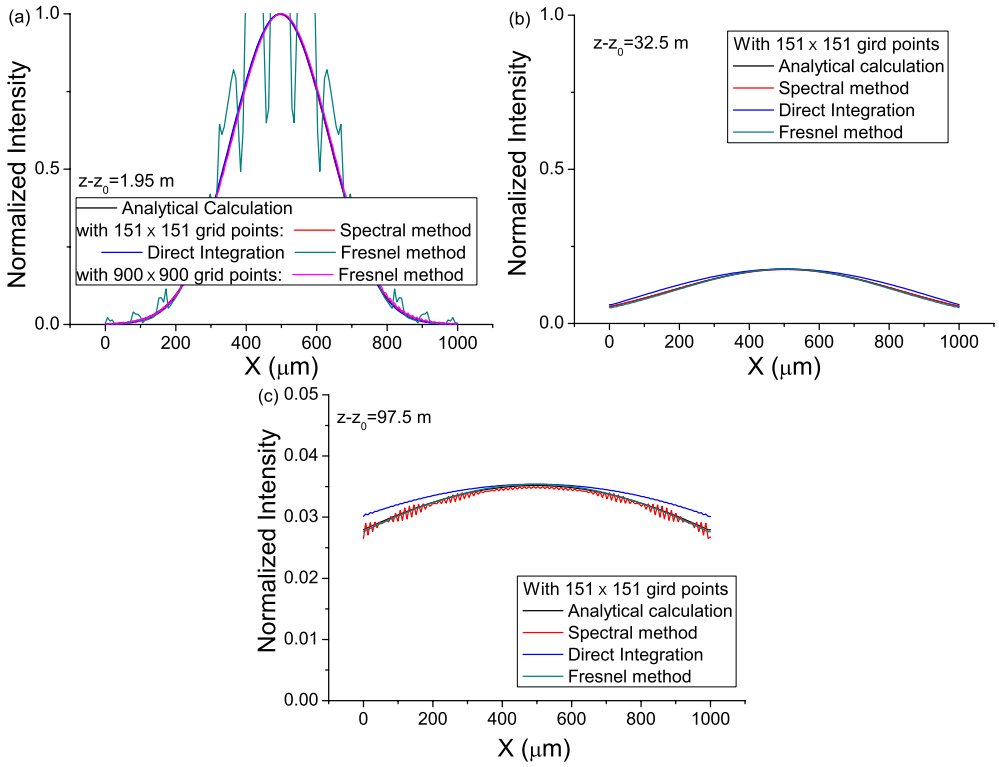

Figure 16: Transverse intensity distribution of a Gaussian aftre propagation using three different methods. The simulation is done by spectral method, method of direct integration and Fresnel method are compared with analytical solution. Plot (a): propation length is 1.95 m, Plot (b): propagation length is 32.5 m and Plot (c): propagation length is 97.5 m.

Appendix B: Back ground knowledges of degree of polarization and Stokes parameter

Polarization is an important property of light. It describes orientation of the oscillations in the plane perpendicular to the wave's direction of propagation. In a Cartesian system the transverse oscillation

of electric field can be divided into orthogonally $x-$ and $y-$ direction, assuming $z-$ is the direction of the wave. Light polarization can be described by either the so-called Coherency matrix or by the Stokes parameters. The concept of degree of polarization P is used to describe a partially polarized light ($0 \leq P \leq 1$), $P = 0$ represents an unpolarized wave and $P = 1$ means that the wave is completely polarized [12].

B.1 The coherency matrix and degree of polarization

The electric component of quasi-monochromatic radiation of a mean frequency ϖ propagated in the z-direction is:

$$E_x(t) = a_1(t)e^{-i[\varpi t - \phi_1(t)]}, \qquad E_y(t) = a_2(t)e^{-i[\varpi t - \phi_2(t)]}. \tag{25}$$

Suppose that the y-component of the electric field is retarded by a phase ϵ with respect to the x-component and that the wave propagates through a slit with an angle θ in the transverse plane with respect to the positive x-direction (which means only the electric component parallel to the slit can be observed). Then the electric field is:

$$E(t;\ \theta,\ \epsilon) = E_x \cos\theta + E_y e^{i\epsilon} \sin\theta. \tag{26}$$

Therefore, the intensity $I(\theta,\ \epsilon)$ is

$$\begin{aligned} &I(\theta,\ \epsilon) = \langle E(t;\ \theta,\ \epsilon) E^*(t;\ \theta,\ \epsilon) \rangle \\ &= J_{xx}\cos^2\theta + J_{yy}\sin^2\theta + J_{xy}e^{i\epsilon}\sin\theta + J_{yx}e^{i\epsilon}\cos\theta, \end{aligned} \tag{27}$$

where superscript $*$ means the complex conjugated value. $J_{xx}, ...$ are the elements of the coherency matrix:

$$J = \begin{pmatrix} \langle E_x E_x^* \rangle & \langle E_x E_y^* \rangle \\ \langle E_y E_x^* \rangle & \langle E_y E_y^* \rangle \end{pmatrix} = \begin{pmatrix} \langle a_1^2 \rangle & \langle a_1 a_2 e^{i(\phi_1 - \phi_2)} \rangle \\ \langle a_1 a_2 e^{-i(\phi_1 - \phi_2)} \rangle & \langle a_2^2 \rangle \end{pmatrix}. \tag{28}$$

In the coherency matrix the parameters a_1, a_2, ϕ_1, ϕ_2 depend on time and $\langle ... \rangle$ refers to averaging over time. The trace of this matrix is equal to the total intensity of the light

$$\mathtt{Tr} J = J_{xx} + J_{yy} = \langle E_x E_x^* \rangle + \langle E_y E_y^* \rangle. \tag{29}$$

For a completely unpolarized wave, the coherency matrix is:

$$J = \begin{pmatrix} A & 0 \\ 0 & A \end{pmatrix}. \tag{30}$$

For a completely polarized light, the coherency matrix is:

$$J = \begin{pmatrix} B & D \\ D^* & C \end{pmatrix}, \quad BC - DD^* = 0. \tag{31}$$

When two optical waves are superimposed, the total electric field in x and y can be expressed as:

$$\begin{aligned} E_x &= E_{1x} + E_{2x} \\ E_y &= E_{1y} + E_{2y}. \end{aligned} \tag{32}$$

The subscripts 1 and 2 denote to the first and second wave. Therefore the products in Eq. (28) are:

$$\begin{aligned} E_x E_x^* &= E_{1x}E_{1x}^* + E_{1x}E_{2x}^* + E_{2x}E_{1x}^* + E_{2x}E_{2x}^* \\ E_y E_y^* &= E_{1y}E_{1y}^* + E_{1y}E_{2y}^* + E_{2y}E_{1y}^* + E_{2y}E_{2y}^* \\ E_x E_y^* &= E_{1x}E_{1y}^* + E_{1x}E_{2y}^* + E_{2x}E_{1y}^* + E_{2x}E_{2y}^* \\ E_y E_x^* &= E_{1y}E_{1x}^* + E_{1y}E_{2x}^* + E_{2y}E_{1x}^* + E_{2y}E_{2x}^*. \end{aligned} \tag{33}$$

When the amplitude and phase of the two waves are completely independent, the average of the product of their electric components are zero, e.g.

$$\begin{aligned} &\langle E_{1x}E_{2y}^* \rangle = \langle E_{1y}E_{2x}^* \rangle = \langle E_{2x}E_{1y}^* \rangle = \langle E_{2y}E_{1x}^* \rangle = 0 \\ &\langle E_{1x}E_{2x}^* \rangle = \langle E_{1y}E_{2y}^* \rangle = \langle E_{2x}E_{1x}^* \rangle = \langle E_{2y}E_{1y}^* \rangle = 0. \end{aligned} \tag{34}$$

Then

$$\begin{array}{l}\langle E_x E_x^*\rangle = \langle E_{1x} E_{1x}^*\rangle + \langle E_{2x} E_{2x}^*\rangle \\ \langle E_y E_y^*\rangle = \langle E_{1y} E_{1y}^*\rangle + \langle E_{2y} E_{2y}^*\rangle \\ \langle E_x E_y^*\rangle = \langle E_{1x} E_{1y}^*\rangle + \langle E_{2x} E_{2y}^*\rangle \\ \langle E_y E_x^*\rangle = \langle E_{1y} E_{1x}^*\rangle + \langle E_{2y} E_{2x}^*\rangle .\end{array} \tag{35}$$

According to Eq. (28)

$$J_{ij} = J_{ij}^{(1)} + J_{ij}^{(2)}, \quad i,j = x,y, \tag{36}$$

where the superscripts 1 and 2 refer to the first and second optical beam.

It can also be shown that if several independent waves are superposed, the coherency matrix of them is equal to the sum of the coherency matrix of the individual waves (similar description will be shown for the Stokes parameters):

$$J_{xy} = \sum_n J_{xy}^{(n)}. \tag{37}$$

Thus the coherency matrix can be divided in the form of sum of two individual matrices, one of them represents a completely unpolarized wave $J^{(1)}$ and the other represents a polarized wave $J^{(2)}$:

$$\begin{array}{c} J = J^{(1)} + J^{(2)} = \begin{pmatrix} J_{xx} & J_{xy} \\ J_{yx} & J_{yy} \end{pmatrix} \\ J^{(1)} = \begin{pmatrix} A & 0 \\ 0 & A \end{pmatrix} \quad J^{(2)} = \begin{pmatrix} B & D \\ D^* & C \end{pmatrix}, \quad BC - DD^* = 0. \end{array} \tag{38}$$

Therefore the total intensity of the wave I_{tot} and the completely polarized part intensity I_{pol} can be individually calculated:

$$\begin{array}{c} I_{tot} = \mathtt{Tr}J = J_{xx} + J_{yy} \\ I_{pol} = \mathtt{Tr}(J^{(2)}) = B + C = \sqrt{(J_{xx} + J_{yy})^2 - 4|J|}. \end{array} \tag{39}$$

The degree of polarization is defined as the ratio of the intensity of the completely polarized wave and that of the total intensity. Hence, the value can be calculated by the coherency matrix:

$$P = \frac{I_{pol}}{I_{tot}} = \sqrt{1 - \frac{4|J|}{(J_{xx} + J_{yy})^2}}. \tag{40}$$

B.2 Stokes parameters

Stokes parameters are generally used to describe the polarization. It includes four real elements $S_0,\ S_1,\ S_2,\ S_3$ instead of the four complex elements in the coherency matrix. The Stokes parameters are defined as:

$$S_0 = \langle a_1^2\rangle + \langle a_2^2\rangle, \quad S_1 = \langle a_1^2\rangle - \langle a_2^2\rangle, \quad S_2 = 2\langle a_1 a_2 \cos(\phi_1 - \phi_2)\rangle, \quad S_3 = 2\langle a_1 a_2 \sin(\phi_1 - \phi_2)\rangle . \tag{41}$$

The relation between Stokes parameters and the coherency matrix elements is:

$$\begin{array}{ll} S_0 = J_{xx} + J_{yy} & J_{xx} = \frac{1}{2}(S_0 + S_1) \\ S_1 = J_{xx} - J_{yy} & J_{yy} = \frac{1}{2}(S_0 - S_1) \\ S_2 = J_{xy} + J_{yx} \quad , & J_{xy} = \frac{1}{2}(S_2 + iS_3) \\ S_3 = i(J_{yx} - J_{xy}) & J_{yx} = \frac{1}{2}(S_2 - iS_3). \end{array} \tag{42}$$

Similar to the coherency matrix, if several independent optical fields are superimposed, the Stokes parameters of total field are a superposition of the Stokes parameters of each individual field

$$S_0 = \sum_{i=1}^n S_0^{(i)}, \quad S_1 = \sum_{i=1}^n S_1^{(i)}, \quad S_2 = \sum_{i=1}^n S_2^{(i)}, \quad S_3 = \sum_{i=1}^n S_3^{(i)}. \tag{43}$$

It is easy to express degree of polarization by Stokes parameter:

$$P = \frac{\sqrt{S_1^2 + S_2^2 + S_3^2}}{S_0}. \tag{44}$$

If the optical beam is partially polarized ($0 < P < 1$), the Stokes parameter can be expressed as:

$$S = \begin{pmatrix} S_0 \\ S_1 \\ S_2 \\ S_3 \end{pmatrix} = (1-P)\begin{pmatrix} S_0 \\ 0 \\ 0 \\ 0 \end{pmatrix} + P\begin{pmatrix} S_0 \\ S_1 \\ S_2 \\ S_3 \end{pmatrix}. \tag{45}$$

Stokes parameter can completely describe an optical beams' polarization property. By this expression, the polarization is clear. S_0 represents the total intensity and $S_1,\ S_2,\ S_3$ respectively represent a certain polarization:

$$\begin{pmatrix} S_0 \\ S_1 \\ S_2 \\ S_3 \end{pmatrix} = \begin{pmatrix} 1 \\ 1 \\ 0 \\ 0 \end{pmatrix}_{\texttt{LHP}} \begin{pmatrix} 1 \\ -1 \\ 0 \\ 0 \end{pmatrix}_{\texttt{LVP}} \begin{pmatrix} 1 \\ 0 \\ -1 \\ 0 \end{pmatrix}_{\texttt{L}\pm\texttt{45P}} \begin{pmatrix} 1 \\ 0 \\ 0 \\ -1 \end{pmatrix}_{\texttt{LCP}} \begin{pmatrix} 1 \\ 0 \\ 0 \\ 1 \end{pmatrix}_{\texttt{RCP}}. \tag{46}$$

Where the subscripts represent different polarization status. LHP means horizontal linear, LVP means vertical linear, L±45P mean $\pm 45^o$ linear, LCP means left circle and RCP means right circle.

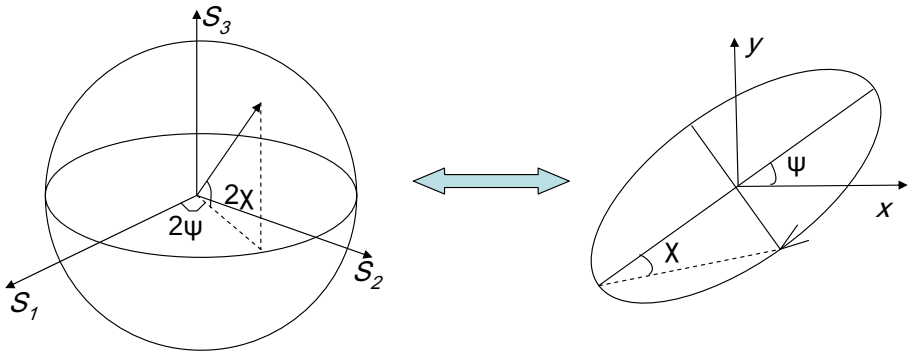

Figure 17: Stokes parameter described by spherical cooredinates (left) and the cylindrical coordinates (right).

The stokes parameters can also be described by spherical coordinates. Fig. 17 shows the expression. The radius of the sphere is the number of S_0. If the vector ends on the sphere surface, it means the light is totally polarized. The origin represents the totally unpolarized wave and the vector inside the sphere is partially polarized. The vector can not exceed the sphere surface which means that $S_1^2 + S_2^2 + S_3^2 \leq S_0^2$. Stokes parameters can be described by the spherical angles ψ and χ as:

$$S_1 = S_0 \cos 2\psi \cos 2\chi, \quad S_2 = S_0 \sin 2\psi \cos 2\chi, \quad S_3 = S_0 \sin 2\chi, \quad 0 < \psi \leq \pi, \ -\tfrac{\pi}{4} < \chi \leq \tfrac{\pi}{4}. \tag{47}$$

In this report we adopt Stokes parameter and the degree of polarization to describe the optical beam polarization.

B.3 Axial phase shifts: the influence of different transporting lengths on the polarization

As shown in Fig. 2, a phase shifter is placed between the two crossed undulators. It is used to fine tune the longitudinal delay of the second wave with respect to the first one. The shift is only one or several

radiation wavelengths. By this means an arbitrary polarization direction, including circular polarization, can be achieved.

In 1D approximation, a $\pi/2$ phase shift corresponds to circular polarization, zero phase shift corresponds to $+45^o$ linear polarization and so on. But the GUOY effect should be taken into accounted in 3D simulation. In vacuum, the paraxial wave can be expressed as a sum of Gauss-Laguerre polynomials:

$$a_s(r,z)e^{i\phi_s(r,z)} = \sum_{p=0}^{\infty} a_p \frac{s_0}{s} L_p(\xi) e^{-(1-i\alpha)\xi/2} e^{-i\zeta_p}. \tag{48}$$

In this equation

$$L_p(\xi) = \sum_{m=0}^{p} (-1)^m C_p^m \frac{\xi^m}{m!}, \tag{49}$$

is the Laguerre polynomial of argument $\xi = 2r^2/s^2$, where s denotes the spot size of the electromagnetic wave, and

$$s = s_0\sqrt{1+\alpha^2}, \quad \alpha = (z-z_0)/z_R, \quad \zeta_p(\alpha) = (2p+1)\ \arctan\alpha, \quad z_R = k_r s_0^2/2\,. \tag{50}$$

On the center point ($r = 0, \xi = 0$) the optical beam phase is only determined by ζ_p. Furthermore setting $p = 0$, the phase shift after a certain distance from the start point is δ:

$$\delta = \arctan\alpha. \tag{51}$$

To evaluate the value of δ, it is needed to determine the Rayleigh length. The spot size $s(z)$ for far field case can be calculated as:

$$s(z) = s_0\sqrt{1+\frac{z^2}{z_R^2}}, \quad z_R = \frac{k_r}{2}s_0^2. \tag{52}$$

In far zone $z >> z_R$, the radiation divergence θ ($\theta = \frac{ds(z)}{dz}$) is:

$$\theta = \frac{ds(z)}{dz} = \frac{s_0}{z_R} = \sqrt{\frac{2}{k_r z_R}}. \tag{53}$$

Therefore if the field divergence can be simulated, the Rayleigh length is known and then the phase shift δ can be calculated.

Another method of evaluating δ is based on Stokes parameters. From Eq. (41), for two identical fields ($a_1(t) = a_2(t),\ \phi_1(t) = \phi_2(t)$), their phase shift is

$$\delta = -(\phi_1 - \phi_2) = -\arctan(S_3/S_2). \tag{54}$$

This implies that the polarization to some extent depends on the field divergence θ. If θ changes significantly from shot to shot, the on-axis phase shift changes as well which in turn means some fluctuation of the polarization.

References

[1] Massimo Altarelli et.al., The European X-Ray Free-Electron Laser, Technical Design Report, ISBN 3-935702-17-5.

[2] H. Kondratenko, E.L. Saldin, Particle Accelerators 10 (1980) 2.

[3] R. Bonifacio, C. Pellegrini, L.M. Narducci, Opt. Commun. 50 (1984) 373.

[4] J. Bahrdt et.al., et.al., Nucl. Instr. and Meth. A 516 (2004) 575.

[5] K.J. Kim, Nucl. Instr. and Meth. 219 (1984) 42.

[6] K.J. Kim, Nucl. Instr. and Meth. 445 (2000) 329.

[7] Yuantao Ding, Zhirong Huang, Phys. Rev. ST. AB. 11 (2008) 030702.

[8] Y. Li, B. Faatz, J. Pflueger, E.A. Saldin, E.L. Schneidmiller, M.V. Yurkov, Study of Controllable Polarization SASE FEL by a crossed-planar Undulator, presented at the European Particle Accelerator Conference 2008, Italy.

[9] S. Reiche, Nucl. Instr. and Meth. **A429** (1999) 243-248.

[10] Y. Li, W. Decking, B. Faatz, J. Pflueger, Proceedings of the FEL09, Aug 23-28, 2009, Liverpool, Great Britain.

[11] Y. Li, W. Decking, B. Faatz, J. Pflueger, submitted to Phys.Rev. ST.

[12] M. Born, E. Wolf, Principles of Optics, 7th ed. (Cambridge U. P., New York, 1999).

[13] William H. Press et.al., Numerical Recipes in FORTRAN, 2nd ed. (Cambridge U. P., New York, 1992).